

PACS numbers: 42.30.Wb; 42.25.Dd; 42.25.Fx
DOI: 10.1070/QE2014v044n08ABEH015495

Calculation of the weighting functions for the reconstruction of absorbing inhomogeneities in tissue by time-resolved optical projections

A.B. Konovalov, V.V. Vlasov

Abstract. **We report a new method for determining the weighting functions to reconstruct absorbing inhomogeneities in tissue by perturbation time-domain diffuse optical tomography using the transmission geometry of a flat layer. The method is based on an analytical approach to the calculation of the weighting functions for a semi-infinite scattering medium and on the use of the original method of an equivalent inverse source in order to obtain weight distributions for the flat layer geometry. The correctness of the proposed method of the weighting function calculation is evaluated by a numerical experiment on the reconstruction of absorbing inhomogeneities. It is shown that the perturbation reconstruction model based on the proposed weighting function calculation method allows the inhomogeneities smaller than 0.3 cm and ~0.4 cm, located respectively in the transverse and longitudinal directions to the probe light direction, to be resolved in the centre of an 8-cm-thick object.**

Keywords: *diffuse optical tomography, perturbation reconstruction model, weighting function, absorbing inhomogeneity, time-resolved optical projection, transverse and longitudinal spatial resolution.*

1. Introduction

The last decade has seen a rapid development of the methods of diffuse optical tomography (DOT) of tissues [1–14]. The most accurate and promising are nonlinear iterative methods [2, 5, 6, 10, 11, 13–17], based on multi-step linearization of forward and inverse DOT problems and on alignment of the weight matrix, which is responsible for the reconstruction of diffusion tomograms, at each step. However, despite the rapid progress of computer technology, reconstruction and visualisation of spatial distributions of optical and functional parameters of tissue using these methods incur heavy computational burden – from tens of minutes to several hours [2, 17], which cannot fully meet the requirements of modern medical diagnosis. For this reason, researchers continue to pay serious attention to the development of approximate methods of DOT reconstruction, which are usually inferior to the accuracy of nonlinear methods, but provide images almost in real time. Among the approximate methods, perturbation methods [18–22] and methods for localisation of optical inhomogeneities [23–26] are most widely used. Perturbation methods neglect nonlinearity of forward and inverse DOT problems; as a result, the inverse problem reduces to a time saving, single inversion of a system of linear algebraic equations. Perturbation methods can compete in accuracy with nonlinear methods in the case when optical inhomogeneities are small in size and amplitude. Localisation methods rely on fitting techniques, which are based on a comparison of experimental data with calculations obtained on the basis of the analytical solution of the transport or diffusion equation for a homogeneous medium with a spherical inhomogeneity. These methods do not actually give information about the real shape of the inhomogeneity, but are used with some success in experimental clinical trials to determine the optical parameters of localised tumours [25, 27–30]. In recent years the range of approximate DOT methods has expanded significantly. We are pleased to note that a substantial contribution to this expansion has been made by Russian researchers. As examples, we can single out the following approximate DOT methods developed by Russian scientists: nonlinear statistical methods [31–34], the method of photon average trajectories [35–42], the inverse method using Tikhonov regularisation with non-negative components [43, 44], and the inhomogeneity localisation method based on the use of late-arriving photons [45–47].

In this paper, we develop the perturbation reconstruction model proposed by Lyubimov for the case of time-domain DOT (Lyubimov's model) [35–37, 48]. The uniqueness of this model is that, instead of such integral data as integrated intensity, average time of flight of photons, results of Laplace and Mellin–Laplace transforms, etc. (see, for example, [15]), diffusion tomograms are reconstructed using time-resolved optical projections [42, 48, 49]. These projections are measured for only one time-gating delay and minimise the spatial resolution of the method. More recently, we have shown [49] that if we take into account the contribution of each point of a scattering object to the signal and use total banana-shaped distributions of photon trajectories during the reconstruction, Lyubimov's model allows a 2.5–3-mm inhomogeneity to be resolved in the centre of an 8-cm-thick object. Such values are not only equal but even surpass the spatial resolution of nonlinear multi-step DOT methods [50]. According to Lyubimov's model, the inverse DOT problem in the case of absorbing inhomogeneities is reduced to solving a linear Fredholm integral equation of the 1st kind [37–42, 48, 49]

$$g(\boldsymbol{r}_\mathrm{s}, t_\mathrm{s}, \boldsymbol{r}_\mathrm{d}, t_\mathrm{d}) = \int_V W_{\mu_\mathrm{a}}(\boldsymbol{r}_\mathrm{s}, t_\mathrm{s}, \boldsymbol{r}_\mathrm{d}, t_\mathrm{d}, \boldsymbol{r}) \delta\mu_\mathrm{a}(\boldsymbol{r}) \mathrm{d}^3 r, \quad (1)$$

where

A.B. Konovalov, V.V. Vlasov Russian Federal Nuclear Center 'E.I. Zababakhin All-Russian Scientific Research Institute of Technical Physics', ul. Vasil'eva 13, PO Box 245, 456770 Snezhinsk, Chelyabinsk region, Russia;
e-mail: a_konov@mail.vega-int.ru, vitaly.vlasov.v@gmail.com

Received 16 March 2014; revision received 17 May 2014
Kvantovaya Elektronika **44** (8) 719–725 (2014)
Translated by I.A. Ulitkin

$$W_{\mu_a}(\boldsymbol{r}_s, t_s, \boldsymbol{r}_d, t_d, \boldsymbol{r}) = c\int_{t_s}^{t_d} P[\boldsymbol{r}, t\,|\,(\boldsymbol{r}_s, t_s) \to (\boldsymbol{r}_d, t_d)]\mathrm{d}t. \quad (2)$$

Here, $(\boldsymbol{r}_s, t_s)$ and $(\boldsymbol{r}_d, t_d)$ are space-time points, which determine the position of the source and detector on the boundary of a scattering object of volume V; $g(\boldsymbol{r}_s, t_s, \boldsymbol{r}_d, t_d)$ is the time-resolved optical projection; $W_{\mu_a}(\boldsymbol{r}_s, t_s, \boldsymbol{r}_d, t_d, \boldsymbol{r})$ is the weighting function, which takes into account the contribution from each object point to the value of $g(\boldsymbol{r}_s, t_s, \boldsymbol{r}_d, t_d)$; $\delta\mu_a(\boldsymbol{r})$ is the local spatial perturbation of the absorption coefficient μ_a; c is the velocity of light in the object; and $P[\boldsymbol{r}, t\,|\,(\boldsymbol{r}_s, t_s) \to (\boldsymbol{r}_d, t_d)]$ is a function that has the meaning of the conditional probability density that a photon migrating from point $(\boldsymbol{r}_s, t_s)$ to point $(\boldsymbol{r}_d, t_d)$ at some intermediate instant of time t will reach the point $\boldsymbol{r} \in V$.

To determine $W_{\mu_a}(\boldsymbol{r}_s, t_s, \boldsymbol{r}_d, t_d, \boldsymbol{r})$ in the case of the flat layer geometry and its 2D analogue (rectangular geometry), we employed [48] a hybrid analytical-numerical approach based on the use of analytical relations for Green's function of the nonstationary diffusion equation and on the numerical integration of expression (2). In this paper, we propose an alternative method for calculating the weighting function $W_{\mu_a}(\boldsymbol{r}_s, t_s, \boldsymbol{r}_d, t_d, \boldsymbol{r})$. This method assumes its analytical calculation for the case of a half-space in 3D and 2D geometries (Section 2), and then the use of the original method of an equivalent inverse source in order to find the weighting functions for the flat layer transmission geometry and transmission rectangular geometry (Section 3). In Section 4 we present the results of numerical experiments on the reconstruction of rectangular scattering objects with absorbing inhomogeneities. These results allow us to estimate the ultimate resolution of the method in the transverse and longitudinal directions with respect to the direction of the probe light and to confirm the correctness of the relations obtained for the weighting functions.

2. Weighting functions in a half-space

Lyubimov et al. [37] found that the probability density $P[\boldsymbol{r}, t\,|\,(\boldsymbol{r}_s, t_s) \to (\boldsymbol{r}_d, t_d)]$ can be determined using the diffusion approximation of the transport equation. To calculate numerically the weighting functions $W_{\mu_a}(\boldsymbol{r}_s, t_s, \boldsymbol{r}_d, t_d, \boldsymbol{r})$, we used [48] the Robin boundary condition [6, 15], which is rightly regarded as the most accurate in the description of photon migration near the boundaries of a scattering object. However, the results of studies [42], where we compared the Dirichlet and Robin boundary conditions, have shown that in the case when the medium represents a half-space, the choice of the boundary condition has little effect on the accuracy of calculation of such statistical characteristics of photon distributions as conditional probability density $P[\boldsymbol{r}, t\,|\,(\boldsymbol{r}_s, t_s) \to (\boldsymbol{r}_d, t_d)]$, average trajectory of photons and standard deviation of photons from the average trajectory. This statement is true at least for relatively short time-gating delays (usually up to 3000 ps). In calculating analytically $W_{\mu_a}(\boldsymbol{r}_s, t_s, \boldsymbol{r}_d, t_d, \boldsymbol{r})$, the results obtained in [42] allow us to use a simpler Dirichlet boundary condition for which the probability density can be given in the form [35, 36, 40, 42]

$$P[\boldsymbol{r}, t\,|\,(\boldsymbol{r}_s, t_s) \to (\boldsymbol{r}_d, t_d)] = \frac{G(\boldsymbol{r} - \boldsymbol{r}_s, t - t_s)\partial G(\boldsymbol{r}_d - \boldsymbol{r}, t_d - t)/\partial q}{\partial G(\boldsymbol{r}_d - \boldsymbol{r}_s, t_d - t_s)/\partial q}, \quad (3)$$

where $G(\boldsymbol{r}-\boldsymbol{r}', t-t')$ is Green's function of the nonstationary diffusion equation, and $\partial/\partial q$ is a derivative in the direction normal to the medium boundary. The problem of calculating the weighting functions is thus reduced to the integration of (3) over time t according to equation (2).

2.1. 3D case

In the case of a homogeneous half-space $z \geqslant 0$ with a diffusion coefficient D and Dirichlet boundary condition, for Green's function $G(\boldsymbol{r}-\boldsymbol{r}', t-t')$ we have the expression [35]:

$$G(\boldsymbol{r} - \boldsymbol{r}', t - t') = [4\pi Dc(t - t')]^{-3/2}\exp[-\mu_a c(t - t')] \times \left\{\exp\left[-\frac{(x - x')^2 + (y - y')^2 + (z - z')^2}{4Dc(t - t')}\right] - \exp\left[-\frac{(x - x')^2 + (y - y')^2 + (z + z')^2}{4Dc(t - t')}\right]\right\}. \quad (4)$$

Let an instantaneous point source be located at point $\boldsymbol{r}_s(0, 0, z_s)$ with the condition $z_s \gg 1/\mu'_{sc}$ being fulfilled, where μ'_{sc} is the reduced scattering coefficient. Let $t_s = 0$, and let a detector be located at point $\boldsymbol{r}_d(x_d, y_d, 0)$ at the medium boundary $z = 0$. By substituting the corresponding expressions for $G(\boldsymbol{r}-\boldsymbol{r}_s, t-t_s)$, $\partial G(\boldsymbol{r}_d-\boldsymbol{r}, t_d-t)/\partial q$ and $\partial G(\boldsymbol{r}_d-\boldsymbol{r}_s, t_d-t_s)/\partial q$ into (3), we obtain

$$P[\boldsymbol{r}, t\,|\,(\boldsymbol{r}_s, t_s) \to (\boldsymbol{r}_d, t_d)] = (2/z_s)(4\pi Dct)^{-3/2}(1 - t/t_d)^{-5/2} \times \exp\left[-\frac{z_s^2(t_d - t)}{4Dct_d t} - \frac{(x_d^2 + y_d^2)t}{4Dct_d(t_d - t)}\right] \times \exp\left[-x^2\frac{t_d}{4Dct(t_d - t)} + x\frac{x_d}{2Dc(t_d - t)}\right] \times \exp\left[-y^2\frac{t_d}{4Dct(t_d - t)} + y\frac{y_d}{2Dc(t_d - t)}\right] \times \exp\left[-z^2\frac{t_d}{4Dct(t_d - t)}\right]z\,\mathrm{sh}\left(z\frac{z_s}{2Dct}\right). \quad (5)$$

A similar expression was obtained in [40, 42] for a detector located at point $\boldsymbol{r}_d(x_d, 0, 0)$. After substituting (5) into (2) and changing the variable $\alpha = t/(t_d - t)$, we obtain

$$W_{\mu_a}(\boldsymbol{r}_s, t_s, \boldsymbol{r}_d, t_d, \boldsymbol{r}) = (z/z_s)(4\pi D)^{-3/2}(ct_d)^{-1/2} \times \exp\left(-\frac{x^2 + y^2 + z^2 - xx_d - yy_d}{2Dct_d}\right) \times \left\{\exp\left(\frac{zz_s}{2Dct_d}\right)\int_0^\infty \alpha^{-3/2}(1 + \alpha)^2 \times \exp\left[-\frac{(x - x_d)^2 + (y - y_d)^2 + z^2}{4Dct_d}\alpha - \frac{x^2 + y^2 + (z - z_s)^2}{4Dct_d}\frac{1}{\alpha}\right]\mathrm{d}\alpha - \exp\left(-\frac{zz_s}{2Dct_d}\right) \times \int_0^\infty \alpha^{-3/2}(1 + \alpha)^2\exp\left[-\frac{(x - x_d)^2 + (y - y_d)^2 + z^2}{4Dct_d}\alpha - \frac{x^2 + y^2 + (z + z_s)^2}{4Dct_d}\frac{1}{\alpha}\right]\mathrm{d}\alpha\right\}. \quad (6)$$

Using the identity $\alpha^{-3/2}(1+\alpha)^2 = \alpha^{-3/2} + 2\alpha^{-1/2} + \alpha^{+1/2}$, in the braces of expression (6), instead of two, we obtain six terms, each of which comprises a standard tabulated integral of form [51]

$$\int_0^\infty \xi^{-3/2}\exp(-p\xi - q/\xi)\,\mathrm{d}\xi = \sqrt{\pi/q}\exp(-2\sqrt{pq}),$$

$$\int_0^\infty \xi^{-1/2}\exp(-p\xi - q/\xi)\,\mathrm{d}\xi = \sqrt{\pi/p}\exp(-2\sqrt{pq}), \qquad (7)$$

$$\int_0^\infty \xi^{1/2}\exp(-p\xi - q/\xi)\,\mathrm{d}\xi = \sqrt{\pi}\left(\frac{1}{2}p^{-3/2} + \frac{\sqrt{q}}{p}\right)\exp(-2\sqrt{pq}).$$

After integration, taking into account (7) and some transformations, expression (6) can be written in the following convenient form:

$$W_{\mu_a}(\boldsymbol{r}_s, t_s, \boldsymbol{r}_d, t_d, \boldsymbol{r}) = \frac{z}{4\pi D z_s}\exp\left(\frac{x_d^2 + y_d^2 + z_s^2}{4Dct_d}\right)$$
$$\times\left\{\exp\left[-\frac{(\beta_- + \gamma)^2}{4Dct_d}\right]\left[\frac{1}{\beta_-}\left(1 + \frac{\beta_-}{\gamma}\right)^2 + \frac{2Dct_d}{\gamma^3}\right]\right.$$
$$\left. - \exp\left[-\frac{(\beta_+ + \gamma)^2}{4Dct_d}\right]\left[\frac{1}{\beta_+}\left(1 + \frac{\beta_+}{\gamma}\right)^2 + \frac{2Dct_d}{\gamma^3}\right]\right\}, \qquad (8)$$

where

$$\beta_\pm = \sqrt{x^2 + y^2 + (z \pm z_s)^2} \text{ и } \gamma = \sqrt{(x - x_d)^2 + (y - y_d)^2 + z^2}.$$

2.2. 2D case

In the case of a 2D half-space $y \geqslant 0$, when the source and detector are located at points $\boldsymbol{r}_s(0, y_s)$ and $\boldsymbol{r}_d(x_d, 0)$, respectively, instead of (5) we obtain the expression

$$P[\boldsymbol{r}, t \mid (\boldsymbol{r}_s, t_s) \to (\boldsymbol{r}_d, t_d)] = \frac{2}{y_s}\frac{1}{4\pi Dct}\left(\frac{t_d}{t_d - t}\right)^2$$
$$\times\exp\left[-\frac{y_s^2(t_d - t)}{4Dct_d t} - \frac{x_d^2 t}{4Dct_d(t_d - t)}\right]$$
$$\times\exp\left[-x^2\frac{t_d}{4Dct(t_d - t)} + x\frac{x_d}{2Dc(t_d - t)}\right]$$
$$\times\exp\left[-y^2\frac{t_d}{4Dct(t_d - t)}\right]y\,\mathrm{sh}\left(y\frac{y_s}{2Dct}\right). \qquad (9)$$

After substituting (9) into (2) and changing the variable $\alpha = t/(t_d - t)$ we obtain an analogue of expression (6):

$$W_{\mu_a}(\boldsymbol{r}_s, t_s, \boldsymbol{r}_d, t_d, \boldsymbol{r}) = \frac{y}{4\pi D y_s}\exp\left(-\frac{x^2 + y^2 - xx_d}{2Dct_d}\right)$$
$$\times\left\{\exp\left(\frac{yy_s}{2Dct_d}\right)\int_0^\infty \frac{1+\alpha}{\alpha}\exp\left[-\frac{(x - x_d)^2 + y^2}{4Dct_d}\alpha\right.\right.$$
$$\left. - \frac{x^2 + (y - y_s)^2}{4Dct_d}\frac{1}{\alpha}\right]\mathrm{d}\alpha$$
$$- \exp\left(-\frac{yy_s}{2Dct_d}\right)\int_0^\infty \frac{1+\alpha}{\alpha}\exp\left[-\frac{(x - x_d)^2 + y^2}{4Dct_d}\alpha\right.$$
$$\left.\left. - \frac{x^2 + (y + y_s)^2}{4Dct_d}\frac{1}{\alpha}\right]\mathrm{d}\alpha\right\}. \qquad (10)$$

Here we come to the tabulated integrals [51]

$$\int_0^\infty \xi^{-1}\exp(-p\xi - q/\xi)\,\mathrm{d}\xi = 2K_0(-2\sqrt{pq}),$$
$$\int_0^\infty \exp(-p\xi - q/\xi)\,\mathrm{d}\xi = 2\left(\frac{q}{p}\right)^{1/2}K_1(-2\sqrt{pq}), \qquad (11)$$

where $K_n(\xi)$ is the Macdonald function of the nth order (n = 0, 1). As a result, the expression for the weighting function can be written in the form:

$$W_{\mu_a}(\boldsymbol{r}_s, t_s, \boldsymbol{r}_d, t_d, \boldsymbol{r}) = \frac{y}{2\pi D y_s}\exp\left(\frac{x_d^2 + y_s^2}{4Dct_d}\right)$$
$$\times\left\{\exp\left[-\frac{(\beta_- + \gamma)^2}{4Dct_d}\right]\left[K_0\left(\frac{\beta_-\gamma}{2Dct_d}\right) + \frac{\beta_-}{\gamma}K_1\left(\frac{\beta_-\gamma}{2Dct_d}\right)\right]\right.$$
$$\left. - \exp\left[-\frac{(\beta_+ + \gamma)^2}{4Dct_d}\right]\left[K_0\left(\frac{\beta_+\gamma}{2Dct_d}\right) + \frac{\beta_+}{\gamma}K_1\left(\frac{\beta_+\gamma}{2Dct_d}\right)\right]\right\}, \qquad (12)$$

where $\beta_\pm = \sqrt{x^2 + (y \pm y_s)^2}$ and $\gamma = \sqrt{(x - x_d)^2 + y^2}$.

This result can be simplified if we utilise the asymptotic approximation of the Macdonald function $K_n(\xi) \cong \sqrt{\pi/2\xi}\exp(-\xi)$. Note that in this case the use of the asymptotic approximation is quite justified, because the incorrectness arises only at very small values of x and y and only when the detector is placed at point $\boldsymbol{r}_d(0, 0)$. After simplifications, we obtain the analytical representation for the weighting function, which is an analogue of expression (8):

$$W_{\mu_a}(\boldsymbol{r}_s, t_s, \boldsymbol{r}_d, t_d, \boldsymbol{r}) = \frac{y}{2y_s}\sqrt{\frac{ct_d}{\pi D}}\exp\left(\frac{x_d^2 + y_s^2}{4Dct_d}\right)$$
$$\times\left\{\exp\left[-\frac{(\beta_- + \gamma)^2}{4Dct_d}\right]\left(\frac{1}{\sqrt{\beta_-\gamma}} + \frac{\sqrt{\beta_-}}{\gamma^{3/2}}\right)\right.$$
$$\left. - \exp\left[-\frac{(\beta_+ + \gamma)^2}{4Dct_d}\right]\left(\frac{1}{\sqrt{\beta_+\gamma}} + \frac{\sqrt{\beta_+}}{\gamma^{3/2}}\right)\right\}. \qquad (13)$$

Spatial distributions of (13) are shown in Fig. 1 for the following parameters: c = 0.0214 cm ps^{-1}, D = 0.034 cm and t_d = 1000, 2000 and 3000 ps. The detector D is located at point $\boldsymbol{r}_d$ (4.3 cm, 0). The source S changes the position and is located at points $\boldsymbol{r}_s$(0, 7.7 cm), $\boldsymbol{r}_s$(0, 7.2 cm) and $\boldsymbol{r}_s$(0, 6.7 cm) in cases when the time-gating delay of the detector is 1000, 2000 and 3000 ps, respectively.

3. Weighting functions for the flat layer geometry. Method of an equivalent inverse source

Unlike a semi-infinite medium, a scattering object in the form of a flat layer has obviously not one plane boundary but two. The problem of applicability of the formulas derived above to describe the propagation of light in a flat layer is reduced to determination of a distance between these boundaries, i.e., the layer thickness d. Contini et al. [52] consider that if $d \gg 1/\mu'_{sc}$, the influence of one boundary on the diffusion process of photon migration near the other can be neglected. Furthermore, according to studies [53] we assume that in this case, the nature of changes in the statistical characteristics of the distribution of photons near the source S located on one boundary is the same as that near the detector D located on

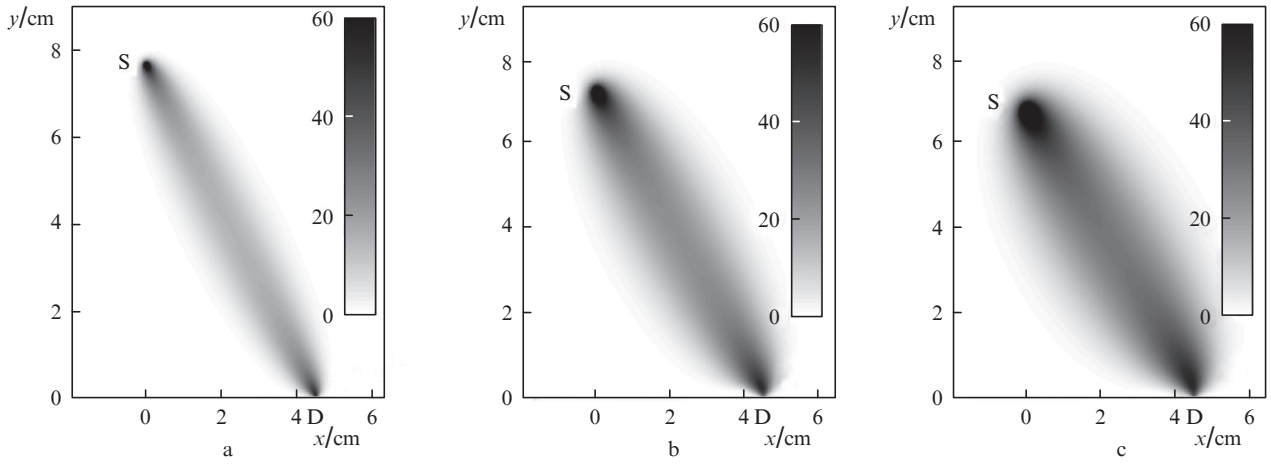

Figure 1. Weighting functions in a 2D half-space for the time-gating delay (a) 1000, (b) 2000 and (c) 3000 ps; the palette scale is graduated in inverse centimetres.

the other boundary (Fig. 2). The above limitation is fully met by optical mammography using the flat layer transmission geometry, since the distance between the plates compressing the breast is usually no less than 5 cm [25–30]. We assume that in our case, the condition $d \geqslant 5$ cm is met.

In this paper, in order to find the weighting functions $W_{\mu_a}(\boldsymbol{r}_s, t_s, \boldsymbol{r}_d, t_d, \boldsymbol{r})$ for the case of the flat layer transmission geometry, we use a technique, which we conditionally called the method of an equivalent inverse source. The method is as follows.

1. We determine the position of the equivalent source S′ (Fig. 2) inside the flat layer, such that, by virtue of the assumptions made, the migration of photons from point S′ to point D with the detector can be considered equivalent to the process of photon migration from S to D in the half of the flat layer with conventional boundaries $z = 0$ and $z = d/2$. For this half we calculate the weighting function by expression (8) or (13).

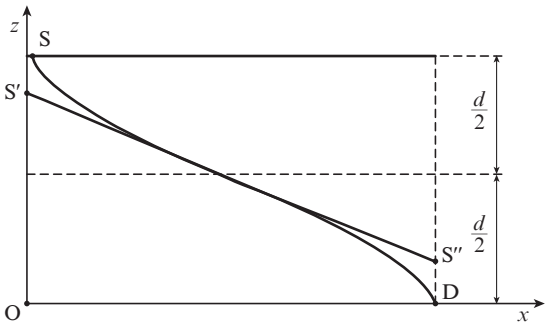

Figure 2. To determination of the position of the equivalent and the equivalent inverse sources (see the text).

2. Similarly to step 1, we find the position of the equivalent inverse source S″ (Fig. 2), such that the migration of photons from point S″ to point S with the detector can be considered equivalent to the process of photon migration from D to S in the other half of the layer with boundaries $z = d/2$ and $z = d$. For this half we also calculate the weighting function by the expressions analogous to formula (8) or (13). These formulas can be easily obtained by following the appropriate coordinate transformation.

3. To obtain the weighting function for the entire flat layer of thickness d, we perform a superposition of 'useful' halves of the weighting functions calculated in steps 1 and 2.

The position of the equivalent source S′ in step 1, as well as the position of the equivalent inverse source S″ in step 2 is found using the previously obtained formulas for the coordinates of the centre of mass of the distribution $P[\boldsymbol{r}, t|(\boldsymbol{r}_s, t_s) \rightarrow (\boldsymbol{r}_d, t_d)]$ that, in fact, describes the average trajectory of photons during their migration from S′ to D and from S″ to S, respectively. These average trajectories are shown in Fig. 2. Derivation of the formulas and the procedure for finding the coordinates $z_{S'}$ and $z_{S''}$ of the equivalent sources S′ and S″ (i.e. distances OS′ and DS″) are described in detail in [40–42]. An

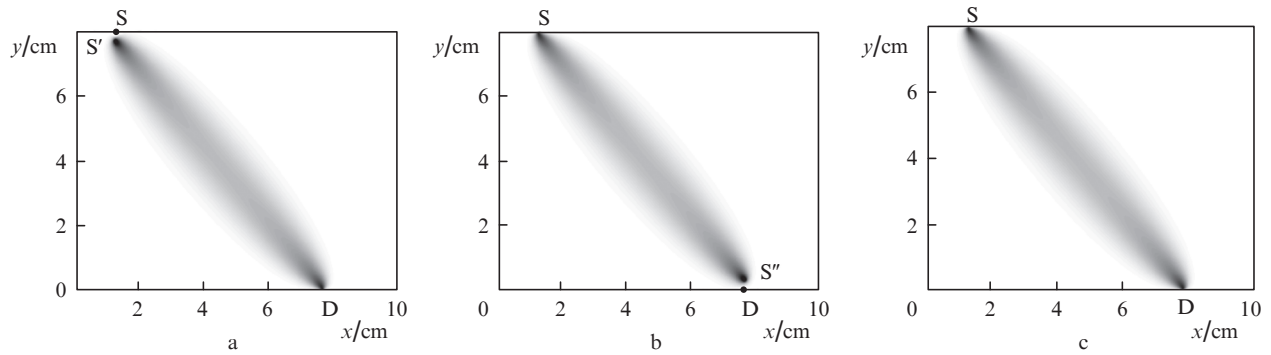

Figure 3. Example of the weighting function calculation by the method of an equivalent inverse source: (a) calculation for the equivalent source, (b) calculation for the equivalent inverse source and (c) superposition of the halves of the weighting functions from Figs 3a and 3b.

example that illustrates the use of the method of an equivalent inverse source in practice is shown in Fig. 3. We considered a rectangular scatterer of size 10 cm× 8 cm, the source S was located at point $\boldsymbol{r}_s$ (1.3 cm, 8 cm), and the detector D – at point $\boldsymbol{r}_d$ (7.7 cm, 0). The optical parameters of the medium were $c = 0.0214$ cm ps^{-1} and $D = 0.034$ cm, and the time-gating delay was $t_d = 1000$ ps. Figure 3a shows the result of calculation for the equivalent source (step 1), Fig. 3b – the result of calculation for the equivalent inverse source (step 2), and Fig. 3c – the result of superposition of the halves of the weighting functions (step 3). Similarly, we can calculate the weighting functions for all positions of the sources and detectors selected for the space-dependent measurements of the optical signal in order to subsequently reconstruct absorbing inhomogeneities.

It should be noted that we used the above described method for the first time. Previously [48, 49], the weighting function in the half-space was determined numerically only for the equivalent source, i.e., only 'direct' calculations were performed. Then the 'useful' half of the distribution obtained was displayed centrally symmetric in order to find the weighting function for the flat layer geometry. In this case, the computational error in the vicinity of the source S reached 10%. To compensate for the error we had to use empirical approaches that require additional time-consuming resources. The method of the equivalent inverse source is free from such drawbacks.

4. Numerical experiment on the reconstruction of absorbing inhomogeneities

4.1. Experimental

To assess the correctness of the calculation of the weighting functions by the method described in Sections 2 and 3, we stage a numerical experiment on the reconstruction of 10× 8 cm scattering rectangular objects with spherical absorbing inhomogeneities. In this paper, we examine for the first time the spatial resolution not only in the direction perpendicular to the direction of the probe light, but also longitudinal (depth) resolution, which, as is known [54], is the most critical in the case of the flat layer geometry. To evaluate the resolution, we use four objects, each of which comprises four spherical absorbing inhomogeneities of the same diameter in the central region. The inhomogeneities are spaced apart so that their centres are arranged at vertices of a square with sides equal to two diameters. The diameters of the inhomogeneities of different objects are 0.3, 0.5, 0.7 and 0.9 cm. The optical properties of the objects are as follows: $c = 0.0214$ cm ps^{-1}, $D = 0.034$ cm and $\mu_a = 0.05$ cm^{-1}. The corresponding reduced scattering coefficient and the absorption coefficients of the inhomogeneities are $\mu'_{sc} = 10$ cm^{-1} and $\mu_a = 0.075$ cm^{-1}, respectively. These values of the optical parameters are characteristic of breast tissue (see, for example, [17, 25, 27–30]). In the numerical experiment we use 32 sources and 32 detectors. The sources and detectors are arranged on opposite sides of the object and alternate with each other with the same step. Because we study the transmission regime, the couplings between the sources and detectors on the same face are ignored. Thus, the number of useful couplings, which are used for the reconstruction, is 32×16.

In order to simulate the measured data by the finite element method we solve the nonstationary diffusion equation with an instantaneous point source. The temporal point-spread functions $\Gamma(\boldsymbol{r}_s, t_s, \boldsymbol{r}_d, t)$ for each source–detector pair are calculated as photon fluxes at the boundaries of the objects in accordance with Fick's law [55]. Time-resolved optical projections are calculated for the time-gating delay t_d = 1000 ps by the formula

$$g(\boldsymbol{r}_s, t_s, \boldsymbol{r}_d, t_d) = -\log \frac{\Gamma(\boldsymbol{r}_s, t_s, \boldsymbol{r}_d, t)\big|_{t=t_d}}{\Gamma_0(\boldsymbol{r}_s, t_s, \boldsymbol{r}_d, t)\big|_{t=t_d}}. \quad (14)$$

Here, the subscript '0' refers to a homogeneous scattering object that is not perturbed by the presence of absorbing inhomogeneities. For the reconstruction we use a discrete model in which the problem is reduced to solving a system of linear algebraic equations

$$\boldsymbol{g} = \boldsymbol{W} \times \boldsymbol{f}, \quad (15)$$

where $\boldsymbol{g} = \{g_i\}$ is the vector of time-resolved optical projections; $\boldsymbol{W} = \{W_{ij}\}$ is the matrix of the weighting coefficients, which is obtained by sampling and combining the weighting functions calculated for all the useful couplings between the source and the detector; and $\boldsymbol{f} = \{f_j\}$ is the vector of discrete values of the reconstructed function. For the inversion of system (15) we use a well-studied modified multiplicative algebraic reconstruction technique [40–42, 48, 49]. All four objects are reconstructed on a sufficiently fine grid (187×147) at low values of the control parameter responsible for the rate of convergence of the iterative process. Therefore, the regularised solution is reached only after a considerable number of iterations (typically 5000–10000).

4.2. Results of the reconstruction and their analysis

Figure 4 shows the results of the reconstruction of the four objects to assess the spatial resolution. They are presented in the form of 2D images (Fig. 4a), and 3D plots of the function $\delta\mu_a(\boldsymbol{r})$ (Fig. 4b). Shown only are the central parts of the tomograms measuring 5×4 cm. It can be seen that the resolution limit in the direction perpendicular to the direction of the probe light (transverse resolution) is not limited to the value of 0.3 cm, which is consistent with estimates obtained in [49]. In the longitudinal direction (longitudinal resolution), inhomogeneities of size 0.3 cm are generally not resolved, and inhomogeneities of size 0.5 cm are reconstructed with 65% contrast. i.e., the lateral resolution limit is between 0.3 and 0.5 cm, and likely close to 0.4 cm.

Note that the computation rate at this stage of research is not optimised. The time needed to reconstruct a single image on an Intel PC (1.7-GHz Pentium 4, 512-MB RAM) in MATLAB is from two to three hours. The computation rate can be increased if use is made of a software environment faster than MATLAB, of the methods for the adaptive control of the convergence rate, and of adaptive grid technology. Of particular interest (as was pointed out in [49]) is the application of an object-oriented programming to the parallelization of the reconstruction algorithm on graphics processing units. In this case, the gain in the computation rate can achieve two or more orders of magnitude [56].

5. Conclusions

We report an original method for calculating the weighting functions to reconstruct absorbing inhomogeneities of tissue

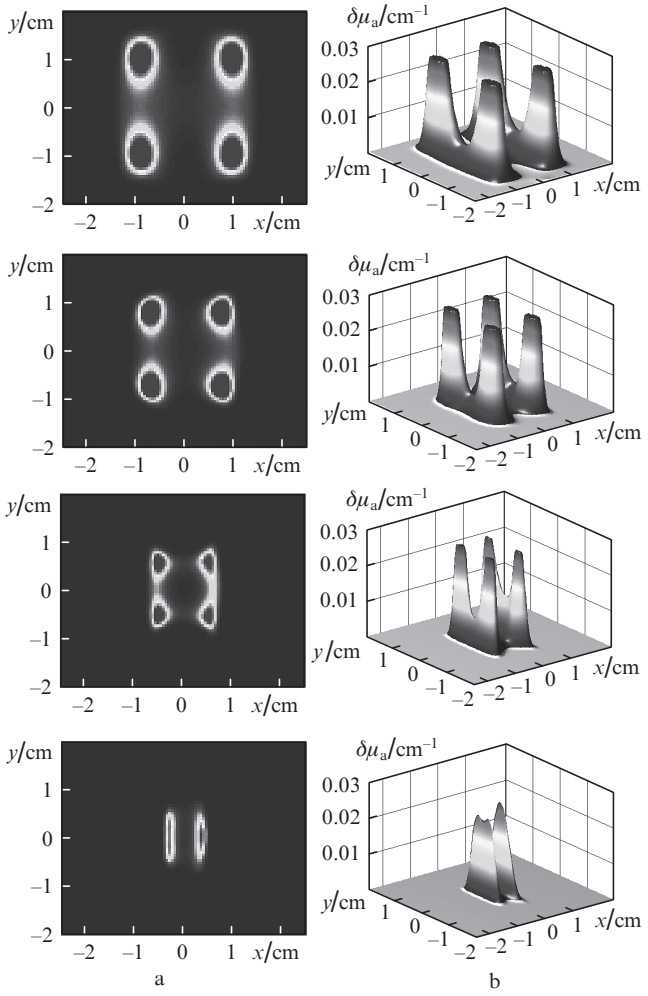

Figure 4. Results of the reconstruction of objects with absorbing inhomogeneities. The diameters of the visualised inhomogeneities (from top to bottom) are equal to 0.9, 0.7, 0.5 and 0.3 cm, respectively.

by time-resolved optical projections using the perturbation model proposed by Lyubimov. The method involves an exact analytical calculation of the weighting functions for the half-space geometry and then the utilisation of the original method of an equivalent inverse source in order to obtain weight distributions for the flat layer transmission geometry. To confirm the correctness of the formulas derived and weighting functions obtained, we have performed a numerical experiment on the reconstruction of rectangular scattering objects with absorbing inhomogeneities. Within the framework of this experiment, the spatial resolution of the method is studied in the transverse and longitudinal directions with respect to the direction of the probe light. It is shown that in the centre of an 8-cm-thick object the transverse resolution is better than 0.3 cm, and the longitudinal resolution is close to 0.4 cm.

In our opinion, Lyubimov's perturbation reconstruction model using time-resolved optical projections and the proposed method of calculation of the weighting functions can be recommended for practical applications, for example, in optical mammography.

Acknowledgements. The authors are grateful to V.V. Lyubimov without whose theoretical studies the publication of this paper would be impossible.

References

1. Gibson A., Hebden J.C., Arridge S.R. *Phys. Med. Biol.*, **50**, R1 (2005).
2. Schweiger M., Arridge S.R., Nissilä I. *Phys. Med. Biol.*, **50**, 2365 (2005).
3. Wang L.V., Wu H.I. *Biomedical Optics: Principles and Imaging* (New Jersey: John Wiley & Sons, 2007).
4. Jacques S.L., Pogue B.W. *J. Biomed. Opt.*, **13**, 041302 (2008).
5. Dehghani H., Eames M.E., Yalavarthy P.K., Davis S.C., Srinivasan S., Carpenter C.M., Pogue B.W., Paulsen K.D. *Commun. Numer. Methods Eng.*, **25**, 711 (2008).
6. Arridge S.R., Schotland J.C. *Inverse Problems*, **25**, 123010 (2009).
7. Durduran T., Choe R., Baker W.B., Yodh A.G. *Rep. Prog. Phys.*, **73**, 076701 (2010).
8. Tuchin V.V. *Lazery i volokonnaya optika v biomeditsinskikh issledovaniyakh* (Lasers and Fibre Optics in Biomedical Research) (Moscow: Fizmatlit, 2010).
9. Li M., Zhang Y., Bai J. *J. Healthcare Eng.*, **1**, 477 (2010).
10. Arridge S.R. *Phil. Trans. R. Soc. A*, **369**, 4558 (2011).
11. Soloviev V.Y., Arridge S.R. *Biomed. Opt. Express*, **2**, 440 (2011).
12. O'Sullivan T.D., Cerussi A.E., Cuccia D.J., Tromberg B.J. *J. Biomed. Opt.*, **17**, 071311 (2012).
13. Prakash J., Yalavarthy P.K. *Med. Phys.*, **40**, 033101 (2013).
14. Prakash J., Shaw C.B., Manjappa R., Kanhirodan R., Yalavarthy P.K. *IEEE J. Sel. Top. Quantum Electron.*, **20**, 6800609 (2014).
15. Arridge S.R. *Inverse Problems*, **15**, R41 (1999).
16. Hielscher A.H., Klose A.D., Hanson K.M. *IEEE Trans. Med. Imag.*, **18**, 262 (1999).
17. Enfield L.C., Gibson A.P., Everdell N.L., et al. *Appl. Opt.*, **46**, 3628 (2007).
18. Kak A.C., Slaney M. *Principles of Computerized Tomographic Imaging* (New York: IEEE Press, 1988).
19. Feng S., Zeng Z.-A., Chance B. *Appl. Opt.*, **34**, 3826 (1995).
20. Arridge S.R. *Appl. Opt.*, **34**, 7395 (1995).
21. Markel V.A., Schotland J.C. *J. Opt. Soc. Am. A*, **18**, 1336 (2001).
22. Markel V.A., Schotland J.C. *Phys. Rev. E.*, **70**, 056616 (2004).
23. Boas D.A., O'Leary M.A., Chance B., Yodh A.G. *Proc. Natl. Acad. Sci. USA*, **91**, 4887 (1994).
24. Fantini S., Walker S.A., Franceschini M.A., et al. *Appl. Opt.*, **37**, 1982 (1998).
25. Grosenick D., Wabnitz H., Rinneberg H., Moesta K.T., Schlag P.M. *Appl. Opt.*, **38**, 2927 (1999).
26. Bai J., Gao T., Ying K., Chen N. *J. Biomed. Opt.*, **10**, 024024 (2005).
27. Grosenick D., Moesta K.T., Wabnitz H., et al. *Appl. Opt.*, **42**, 3170 (2003).
28. Grosenick D., Wabnitz H., Moesta K.T., et al. *Phys. Med. Biol.*, **49**, 1165 (2004).
29. Taroni P., Danesini G., Torricelli A., et al. *J. Biomed. Opt.*, **9**, 464 (2004).
30. Taroni P., Torricelli A., Spinelli L., et al. *Phys. Med. Biol.*, **50**, 2469 (2005).
31. Chursin D.A., Shuvalov V.V., Shutov I.V. *Kvantovaya Elektron.*, **29** (1), 83 (1999) [*Quantum Electron.*, **29** (10), 921 (1999)].
32. Shuvalov V.V., Chursin D.A., Shutov I.V. *Laser Phys.*, **11**, 636 (2001).
33. Tret'yakov E.V., Shuvalov V.V., Shutov I.V. *Kvantovaya Elektron.*, **31** (12), 1095 (2001) [*Quantum Electron.*, **31** (12), 1095 (2001)].
34. Kuratov A.S., Rudenko V.N., Shuvalov V.V. *Kvantovaya Elektron.*, **44** (7), 652 (2014) [*Quantum Electron.*, **44** (7), 652 (2014)].
35. Lyubimov V.V. *Opt. Spektrosk.*, **80**, 687 (1996).
36. Kravtsenyuk O.V., Lyubimov V.V. *Opt. Spektrosk.*, **89**, 119 (2000).
37. Lyubimov V.V., Kalintsev A.G., Konovalov A.B., et al. *Phys. Med. Biol.*, **47**, 2109 (2002).
38. Konovalov A.B., Lyubimov V.V., Kutuzov I.I., et al. *J. Electron. Imaging*, **12**, 602 (2003).
39. Lyubimov V.V., Konovalov A.B., Kutuzov I.I., Kravtsenyuk O.V., Kalintsev A.G., Murzin A.G., Golubkina O.V., Soms L.N., Yavorskaya L.M. *Opt. Zh.*, **70** (10), 37 (2003).

40. Konovalov A.B., Vlasov V.V., Kalintsev A.G., Kravtsenyuk O.V., Lyubimov V.V. *Kvantovaya Elektron*., **36** (11), 1048 (2006) [*Quantum Electron.*, **36** (11), 1048 (2006)].
41. Konovalov A.B., Vlasov V.V., Mogilenskikh D.V., Kravtsenyuk O.V., Lyubimov V.V. *Kvantovaya Elektron*., **38** (6), 588 (2008) [*Quantum Electron*., **38** (6), 588 (2008)].
42. Konovalov A.B., Vlasov V.V., Lyubimov V.V. *Optik*, **124**, 6000 (2013).
43. Fiks I.I. *Cand. Diss*. (Nizhnii Novgorod, Institute of Applied Physics RAS, 2012).
44. Fiks I.I. DOI: 10.1142/S0219876213500710.
45. Proskurin S.G. *Kvantovaya Elektron*., **41** (5), 402 (2011) [*Quantum Electron*., **41** (5), 402 (2011)].
46. Proskurin S.G., Potlov A.Y. *Photon. Las. Med.*, **2**, 139 (2013).
47. Potlov A.Yu., Proskurin S.G., Frolov S.V. *Kvantovaya Elektron*., **44** (2), 174 (2014) [*Quantum Electron*., **44** (2), 174 (2014)].
48. Konovalov A.B., Vlasov V.V., Uglov A.S., Lyubimov V.V. *Proc. SPIE Int. Soc. Opt. Eng.*, **8088**, 80880T (2011).
49. Konovalov A.B., Vlasov V.V. *Kvantovaya Elektron*., **44** (3), 239 (2014) [*Quantum Electron*., **44** (3), 239 (2014)].
50. Pogue B.W., Davis S.C., Song X., Brooksby B.A., Dehghani H., Paulsen K.D. *J. Biomed. Opt.*, **11**, 033001 (2006).
51. Prudnikov A.P., Brychkov Yu.A., Marichev O.I. *Integrals and Series, Vol. 1: Elementary Functions* (New York: Gordon and Breach, 1986).
52. Contini D., Martelli F., Zaccanti G. *Appl. Opt.*, **36**, 4587 (1997).
53. Volkonskii V.B., Kravtsenyuk O.V., Lyubimov V.V., Mironov E.P., Murzin A.G. *Opt. Spektrosk*., **86**, 299 (1999).
54. Pogue B.W., McBride T.O., Osterberg U.L., Paulsen K.D. *Opt. Express*, **4**, 270 (1999).
55. Duderstadt J.J., Hamilton L.J. *Nuclear Reactor Analysis* (New York: Wiley, 1976).
56. Doronin A., Meglinski I. *Biomed. Opt. Express*, **2**, 2461 (2011).